Solid State Communications 251 (2017) 73–78

Contents lists available at ScienceDirect

Solid State Communications

journal homepage: www.elsevier.com/locate/ssc

Communication

Magnetization plateaus and ground-state phase diagrams of the S=1 Ising model on the Shastry Sutherland lattice

Seyma Akkaya Deviren

Department of Science Education, Education Faculty, Nevsehir Hacı Bektaş Veli University, 50300 Nevşehir, Turkey

ARTICLE INFO

Keywords:
A. Shastry Sutherland lattice
D. Ground-state phase diagrams
D. Magnetization plateaus
D. Spin-1

ABSTRACT

In this research, we have investigated the magnetic properties of the spin-1 Ising model on the Shastry Sutherland lattice with the crystal field interaction by using the effective-field theory with correlations. The effects of the applied field on the magnetization are examined in detail in order to obtain the magnetization plateaus, thus different types of magnetization plateaus, such as 1/4, 1/3, 1/2, 3/5, 2/3 and 7/9 of the saturation, are obtained for strong enough magnetic fields (h). Magnetization plateaus exhibit single, triple, quintuplet and sextuple forms according to the interaction parameters, hence the magnetization plateaus originate from the competition between the crystal field (D) and exchange interaction parameters (J, J'). The ground-state phase diagrams of the system are presented in three varied planes, namely (h/J, J'/J), (h/J, D/J) and (D/J, J'/J) planes. These phase diagrams display the Néel (N), collinear (C) and ferromagnetic (F) phases for certain values of the model parameters. The obtained results are in good agreement with some theoretical and experimental studies.

1. Introduction

Shastry Sutherland (S-S) model provides opportunity to investigate frustrated spin systems, which exhibit remarkable magnetic behaviors and have attracted a widespread interest. The S-S lattice, as a frustrated quantum antiferromagnetic model with an exact ground state, was first introduced by Shastry and Sutherland in 1980s [1]. This lattice attracted extensive attention after its experimental realization in the material $SrCu_2(BO_3)_2$[2], since a sequence of magnetization (m) plateaus at fractional values of the saturated magnetization (m_S) (m/m_S =1/3, 1/4 and 1/8) have been experimentally observed in this material [3,4]. After a while, similar magnetization behavior has also been seen in rare-earth tetraborides RB_4 (R=Tb, Dy, Ho, Tm etc.), the magnetic ions of these compounds located on a lattice, which is topologically equivalent to the SSL. For example, for ErB_4 the magnetization plateaus (MP) has been found at m/m_S=1/2 [5,6], for TbB_4 at m/m_S=1/2, 4/9, 1/3, 2/9, and 7/9 [7] and for HoB_4 at m/m_S=1/3, 4/9 and 3/5 [6], for TmB_4 at m/m_S=1/2, 1/7, 1/8, 1/9 [8].

The Shastry Sutherland lattice (SSL) was widely studied theoretically by using various approaches on S=1/2 moments; for example, by using the tensor renormalization group approach [9], the Monte Carlo (MC) algorithm [10–14], the quantum MC [15] and the effective-field theory (EFT) with correlations [16]. Nonequilibrium behaviors of the spin-1/2 Ising model on the SSL are investigated by using the Glauber-type stochastic dynamics [17]. While the magnetic properties of S=1/2 spin systems have been investigated using many different methods, still the magnetic properties of higher spin models (S > 1/2) have not been thoroughly explored as much. Although the RB_4 compounds carry S > 1/2 moments, the local Hilbert space of the localized f-moments in many of these compounds is usually split by a strong single-ion anisotropy into doublets; and the low-energy physics is adequately described by the lowest doublet in terms of an effective S=1/2 XXZ model with strong Ising-like exchange anisotropy [18]. Therefore it is desirable to discuss how the competing exchange interactions affect the ground state properties of a higher-spin (S > 1/2) S-S model.

On the other hand, the crystal field plays an important role for materials consisting of spins with S > 1/2. If the crystal field is strong enough, the energy difference between the split-levels is large. In that case, it is energetically more favourable to put as many electrons as possible into the lower energy level before you start to fill the higher energy levels. Filling all the orbitals in the lower level means that it is an obligation to pair them up (within each orbital) with opposite spins. The effect of pairing the electrons with opposite spin is that there is no addition to the total spin. This results in a low spin state and thus it becomes important to see the effects of the crystal fields for the higher spin. It is also mentioning that we have found a few works about the crystal field effects on the ground state and MP for higher spin (S > 1/2) of the S-S model [18,19]. Lei et. al. have investigated the field-induced magnetic phases of an S=1 XXZ model with single-ion anisotropy and large Ising-like anisotropy on a SSL [18]. Koga et. al.

E-mail address: sadeviren@nevsehir.edu.tr.

http://dx.doi.org/10.1016/j.ssc.2016.12.017
Received 23 June 2016; Received in revised form 28 November 2016; Accepted 22 December 2016
Available online 23 December 2016

have studied quantum phase transitions of the S=1 S-S model with single- ion anisotropy [19]. Richter and Schmidt have examined the exact ground state of a frustrated spin-1 modified S-S model [20].

Thus in this work, we have studied the MPs and ground-state phase diagrams of the spin-1 Ising model within the crystal field (D), magnetic field (h) and exchange interaction parameters (J, J') on the SSL within the EFT with correlations. We have plotted the ground state phase diagram of the model on three different planes, namely (h/J, J'/J), (h/J, D/J) and (D/J, J'/J) planes. Geometrical magnetic frustration, the competition between spin-spin interactions, can lead to new ground states. The effects of the applied field on the magnetizations are examined in detail in order to obtain the MP, and different types of MP, such as 1/4, 1/3, 1/2, 3/5, 2/3 and 7/9 of the saturation, are obtained for strong enough magnetic fields. It is also worth mentioning that the EFT method can incorporate some effects of spin-spin correlations, without introducing mathematical complexity, by using Van der Waerden identities and it can provide results that are quite superior to those obtained by using the mean field approximation (MFA). In this way, up to now, most of the theoretical works have recently treated to study the distinctive magnetic properties of a cylindrical Ising nanowire [21], ultra-thin decorated Ising film [22], mixed spin Ising nanoparticles with core-shell structure [23], cylindrical Ising nanotube [24], diluted spin-1/2 Ising nano cube [25], antiferromagnetic transverse Ising nano island [26], $Fe^{II}Fe^{III}$ bimetallic oxalates [27] and different spin systems [28,29] by using the EFT.

The remainder of this paper is set up as follows. The model and method are represented in Section 2. Section 3 is devoted to the numerical results and discussions. Last section gives a brief summary and conclusion.

2. Model and method

The SSL can be described as a square lattice with antiferromagnetic couplings (J) along the edges of the squares and additional diagonal antiferromagnetic couplings (J') in every second square, as sketched in Fig. 1. In the presence of an applied magnetic field (h) and crystal-field

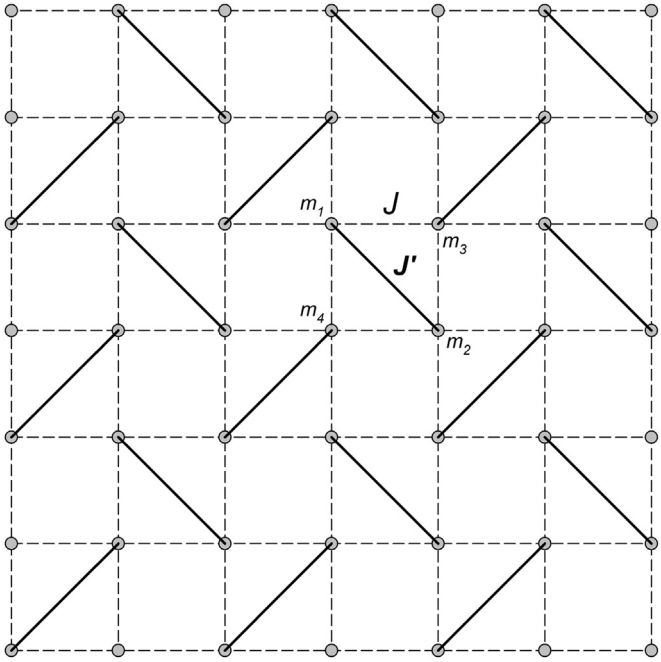

Fig. 1. Schematic representation of the Shastry-Sutherland lattice. The anti-ferromagnetic exchange interaction (J) between all nearest neighbor bonds and additional anti-ferromagnetic exchange interaction (J') between next-nearest neighbor bonds in every second square.

interaction or single-ion anisotropy (D), the Hamiltonian of the spin-1 Ising model on the SSL as studied here is given by

$$H = J\sum_{\langle ij\rangle} s_i\, s_j + J'\sum_{\langle\langle ij\rangle\rangle} s_i\, s_j + D\sum_i s_i^2 - h\sum_i s_i, \tag{1}$$

where s_i takes values $\pm 1, 0$ at each site; $<$ij$>$ indicates a summation over all the square bonds; $\langle\langle ij\rangle\rangle$ runs over all the diagonal bonds.

Now, we calculate effective field equations by using the EFT with correlations, was first introduced by Honmura and Kaneyoshi [30,31] where by a more advanced method is used in dealing with Ising systems than the MFA, because it considers more correlations. The EFT relies on introducing a differential operator into the exact spin correlation function identities obtained by Callen [32] and using the van der Waerden spin identities, which improves substantially on the standard MFA [33]. The EFT method is general and may be applied to systems with any spin value, adapting the van der Waerden identities accordingly. The EFT procedure presents a great versatility and has been recently applied to study the distinctive magnetic properties of complex spin systems such as Refs. [21–29].. The magnetizations ($m_1 = \langle s_1\rangle$, $m_2 = \langle s_2\rangle$, $m_3 = \langle s_3\rangle$ and $m_4 = \langle s_4\rangle$), as seen in Fig. 1, and quadrupole moments ($q_1 = \langle s_1^2\rangle$, $q_2 = \langle s_2^2\rangle$, $q_3 = \langle s_3^2\rangle$ and $q_4 = \langle s_4^2\rangle$), as coupled equations are obtained using the EFT for the SSL as in below:

$$\begin{Bmatrix} m_1 \\ q_1 \end{Bmatrix} = [1 + m_2 \sinh(J'\nabla) + m_2^2(\cosh(J'\nabla) - 1)] \times [1 + m_3 \sinh(J\nabla) + m_3^2(\cosh(J\nabla) - 1)]^2 \times [1 + m_4 \sinh(J\nabla) + m_4^2(\cosh(J\nabla) - 1)]^2 \begin{Bmatrix} f(x+h) \\ g(x+h) \end{Bmatrix}\Big|_{x=0}, \tag{2}$$

$$\begin{Bmatrix} m_2 \\ q_2 \end{Bmatrix} = [1 + m_1 \sinh(J'\nabla) + m_1^2(\cosh(J'\nabla) - 1)] \times [1 + m_3 \sinh(J\nabla) + m_3^2(\cosh(J\nabla) - 1)]^2 \times [1 + m_4 \sinh(J\nabla) + m_4^2(\cosh(J\nabla) - 1)]^2 \begin{Bmatrix} f(x+h) \\ g(x+h) \end{Bmatrix}\Big|_{x=0}, \tag{3}$$

$$\begin{Bmatrix} m_3 \\ q_3 \end{Bmatrix} = [1 + m_1 \sinh(J\nabla) + m_1^2(\cosh(J\nabla) - 1)]^2 \times [1 + m_2 \sinh(J\nabla) + m_2^2(\cosh(J\nabla) - 1)]^2 \times [1 + m_4 \sinh(J'\nabla) + m_4^2(\cosh(J'\nabla) - 1)] \begin{Bmatrix} f(x+h) \\ g(x+h) \end{Bmatrix}\Big|_{x=0}, \tag{4}$$

$$\begin{Bmatrix} m_4 \\ q_4 \end{Bmatrix} = [1 + m_1 \sinh(J\nabla) + m_1^2(\cosh(J\nabla) - 1)]^2 \times [1 + m_2 \sinh(J\nabla) + m_2^2(\cosh(J\nabla) - 1)]^2 \times [1 + m_3 \sinh(J'\nabla) + m_3^2(\cosh(J'\nabla) - 1)] \begin{Bmatrix} f(x+h) \\ g(x+h) \end{Bmatrix}\Big|_{x=0}, \tag{5}$$

where $\nabla = \partial/\partial x$ is a differential operator. The representation of the magnetizations m_1, m_2, m_3 and m_4 are also indicated in Fig. 1. For the magnetizations and quadrupole moments, the functions $f(x+h)$ and $g(x+h)$ are respectively defined by

$$f(x+h) = \frac{2\sinh[\beta(x+h)]}{2\cosh[\beta(x+h)] + \exp(-\beta D)}, \tag{6}$$

$$g(x+h) = \frac{2\cosh[\beta(x+h)]}{2\cosh[\beta(x+h)] + \exp(-\beta D)}, \tag{7}$$

where $\beta = 1/k_B T_A$, T_A is the absolute temperature and k_B is the Boltzmann factor. Since the Hamiltonian of the model has not included the biquadratic exchange interaction parameter in Eq. (1), the thermal behaviors of quadrupole moments have not been investigated. By using the definitions of the order parameters in Eqs. (2)–(5), the total magnetization of per site (m) can be defined as follows:

$$m = \frac{1}{4}(m_1 + m_2 + m_3 + m_4). \quad (8)$$

The numerical results of these equations are given and discussed in the next section.

3. Numerical results and discussions

3.1. Magnetization plateaus (MP)

Now, let us proceed to a discussion of the most interesting results obtained for the spin-1 Ising model on the Shastry-Sutherland lattice (SSL) with the interaction parameters (J, J', h, D), whose magnetic behavior may be fundamentally affected by the geometric frustration triggered by the competing the interaction parameters. For simplicity, we will pass to the dimensionless parameters J'/J, h/J and D/J by normalizing all the interaction parameters with respect to the exchange constant J, which will hereafter serve as the energy unit. The interaction parameter J'/J measures a degree of the geometric frustration inherent in the investigated spin-1 Ising model on the SSL. The order parameters defining the different phases of the spin-1 Ising model on the SSL are:

1) Paramagnetic state (P): $m_1=m_2=m_3=m_4=0.0$,
2) Ferromagnetic state (F): $m_1=m_2=m_3=m_4=1.0$,
3) Neel state (N): $m_1=m_2=-1.0$, $m_3=m_4=1.0$,
4) Collinear state (C): $m_1=m_3=-1.0$, $m_2=m_4=1.0$.

It is also mentioning that the effects of the applied field on the magnetizations are calculated in detail to obtain the different types of MP. By applying the total magnetization reduced with respect to its saturation value (m/m_S) against the external magnetic field, various MP of the saturation are observed. The MP of the SSL is studied at the various values of the interaction parameters (the different values of the J'/J and h/J as examples) in detail because of the distinctive step-like behavior in the magnetic field dependence of the total magnetization, and the obtained results are presented in Fig. 2(a)–(f). In Fig. 2, the magnetization curves display many steps, which denote the existence of the MP on the SSL, m/m_S=1/4, 1/3, 1/2, 3/5, 2/3 and 7/9. As seen in Fig. 2, the six different magnetization topologies are obtained for T=0.0001. (i) Fig. 2(a) is calculated for D/J=0.1 and J'/J=1.0, 1.1 and 1.2. In here, the step-like shapes of the magnetization curves are clearly shown and the half plateau (m/m_S=1/2) is found. The width of the plateau remains stable as the value of J'/J increases, seen in the figure. (ii) The magnetization curves are plotted for D/J=1.0, J'/J =1.0, 1.2 and 1.4, seen in Fig. 2(b). In Fig. 2(b) two new steps, which are located at m/m_S =1/4 and 7/9 of the saturation in addition to m/m_S=1/2, are obtained. (iii) Fig. 2(c) is represented for D/J=1.0, J'/J =0.5, 0.7 and 0.8, the figure shows a similar behavior to Fig. 2(b) but now two more of the MPs, m/m_S=1/3 and 2/3, also exist; hence the system presents quintuplet-plateau (m/m_S =1/4, 1/3, 1/2, 2/3 and 7/9). (iv) We have obtained the richest magnetization curves for D/J=1.0, J'/J =0.4 and 0.45, seen in Fig. 2(d). In this case, these magnetization curves present similar behavior to Fig. 2(c) but now one more of the MP, m/m_S=3/5, also exists; hence the system presents sexuple-plateau (m/m_S=1/4, 1/3, 1/2, 3/5, 2/3 and 7/9). (v) For D/J=1.0, J'/J =0.33, the magnetization curve is similar to Fig. 2(d) but only differs from Fig. 2(d) in that one of the MP, i.e., m/m_S=1/2 disappears, illustrated in Fig. 2(e). The system has five MPs or quintuplet-plateaus (m/m_S=1/4, 1/3, 3/5, 2/3 and 7/9). (vi) The magnetization curves are obtained for D/J =2.0, J'/J =0.6 and 0.8, seen in Fig. 2(f). In Fig. 2(f), the m/m_S is equal to 0.0 (paramagnetic state: $m_1=m_2=m_3=m_4=0.0$) at zero and very low values of the magnetic field as expected, but as the magnetic field increases the magnetic curves change and go to distinctive magnetization plateau, such as m/m_S=1/4, 1/2, 1/3, 1/2, 2/3 and 7/9, respectively, then m/m_S reach to 1.0 (ferromagnetic state: $m_1=m_2=m_3=m_4=1.0$).

Now we compare our results about the MPs with previous studies. There are a few studies about the spin-1 SSL, and the differences or/and similarities between our work and these studies are as follows. For m/m_S=1/3 and 2/3 our results are identical with ones obtained in the magnetic phases in the S=1 SS model [18] and in the exact ground state of a frustrated S=1 SS model [20]. The MP at m/ms=1/4 and 1/2 have been really found in the magnetic phases in the S=1 SS model [18].

3.2. Ground state phase diagrams

The study of the ground state is of central importance for understanding the critical behavior of such systems. The GS phase diagrams of the system are calculated by comparing the values of the energy for different spin configurations and then the ground state configurations are the ones with the lowest energy for given values of D/J, h/J and J'/J for very low values of the temperature, i.e. T=0.0001. We consider the study of the GS phase diagrams of SS model with different combinations of variables in the Hamiltonian, which are indicated by the parameters. As the number of parameters increases, the complexity of the respective diagram will increase. The three, two and one different types of GS phase diagrams have presented in the (h/J, J'/J), (h/J, D/J) and (D/J, J'/J) planes for various values of interaction parameters, seen in the Figs. 3–5, respectively. In the phase diagrams the collinear (−1, 1, −1, 1), the Néel (−1, −1, 1, 1) and ferromagnetic (1, 1, 1, 1) state are observed at the various values of the h/J and J'/J. In addition to these phase regions, the MPs at m/m_S=1/4, 1/3, 1/2, 3/5, 2/3 and 7/9 are obtained.

Fig. 3 represents the GS phase diagrams in the (h/J, J'/J) plane for three different values of D/J, i.e., 1.0, 2.0 and 4.0. From these figures, the following interesting phenomena and main results are observed. (i) Fig. 3(a) is obtained for D/J=1.0. In this phase diagram, the system presents P and F phases and 1/4, 1/3, 1/2, 3/5, 2/3 and 7/9 plateaus for appropriate values of the system parameters. As an interesting point, the system exist three 1/2 plateaus, but their spin structures are markedly different from each other. These plateaus spin structures are (1,0,1,0); (1,1,0,0) and (0,0,1,1) for $J'/J < 0.33$, $0.33 < J'/J < 1.0$ and $J'/J > 1.0$, respectively. As the diagonal interaction increases to $J'/J > 1.0$ the magnetic plateaus 1/3 and 2/3 disappear. When $J'/J > 0.75$ Neel phase emerge at the small values of external magnetic field. (ii) Fig. 3(b) is calculated for D/J=2.0, the topology of the phase diagram is similar to Fig. 3(a) except that the new 1/4 plateau with (0,−1,1,1) spin structure is emerged. It may be related to strong crystal field causing large energy differences between split levels. Moreover the MP start from the h/J=2.0. (iii) Fig. 3(c) is constructed for D/J=4.0, the phase diagram is similar to Fig. 3(b) but only differs from Fig. 3(b) in which the region of P phase enlarged and the MP start from the higher values of the external magnetic field with the increasing values of the crystal field. It is also mentioning that as the values of crystal field become more strong, the areas of the disordered phase regions (paramagnetic phase) increase, as seen in the figure. It is therefore obvious that the crystal field has a very important effect on the ordering of the phase diagrams of the model. These results show that the GS phase diagrams strongly depend on the interaction parameters. The similar phase diagram has been obtained in the S=1 XXZ model with single-ion anisotropy and large Ising-like anisotropy on a SSL [18].

We also calculated the GS phase diagrams of the model in the (h/J, D/J) and (D/J, J'/J) planes and present them in Fig. 4 and Fig. 5, respectively. From these phase diagrams, we have observed following interesting phenomena. (i) Fig. 4 are obtained in the (h/J, D/J) plane for J'/J=1.0 and 0.1 in order to see the effect of the J'. In Fig. 4(a), the GS phase diagram are calculated for J'/J=1.0, and the N, F, P phases and two 1/2 plateaus "(1,−1,1,1) spin structure for small values of the D/J and (1,1,0,0) spin structure for high values of the D/J", two 1/4 plateaus "(0,−1,1,1) spin structure for small values of the D/J and (1,0,0,0) spin structure for high values of the D/J" and 7/9 plateau are seen. (ii) Fig. 4(b) is presented for J'/J=0.1, the phase diagram is

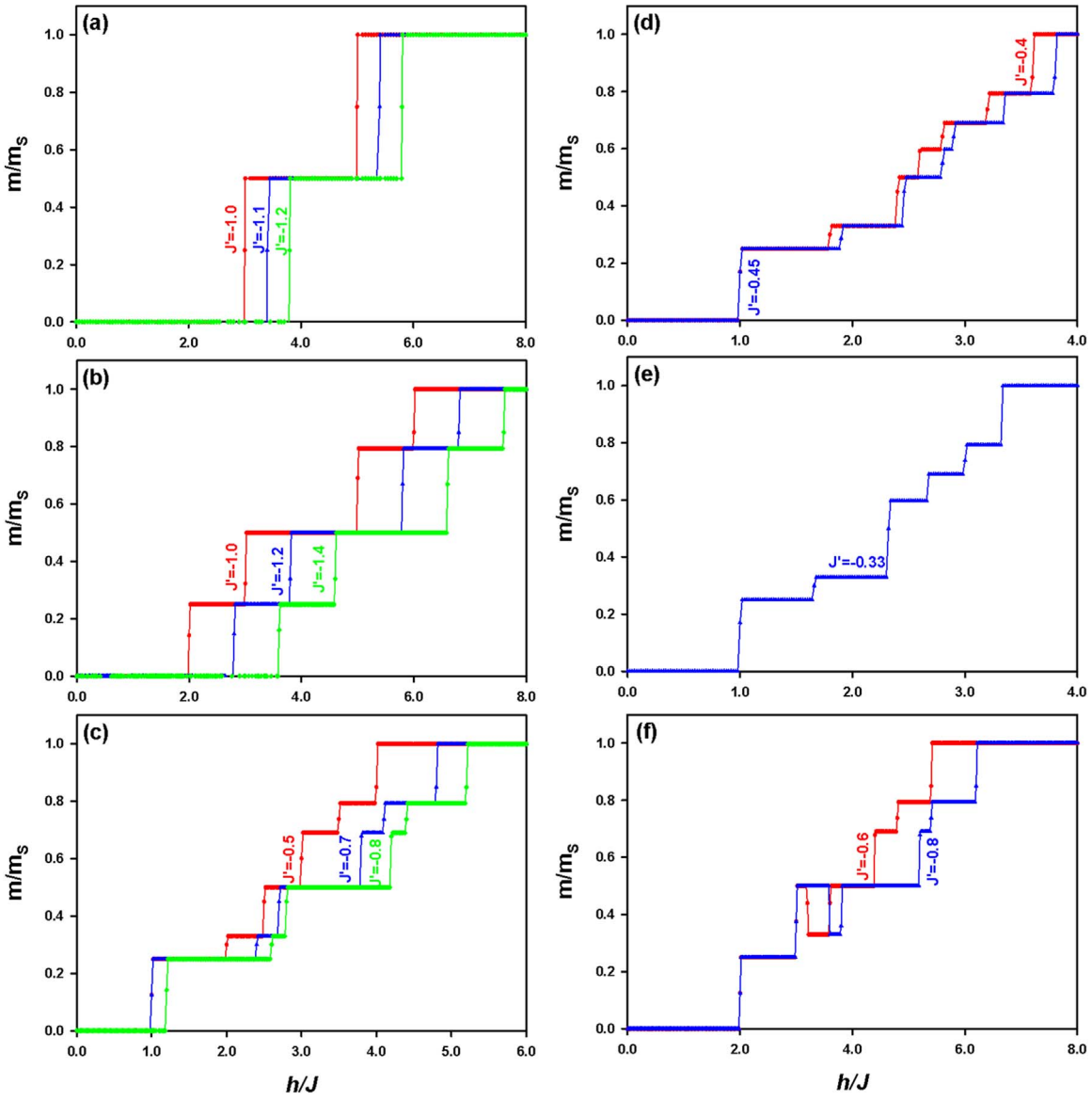

Fig. 2. Magnetization curves at selected values of the ratio of the physical parameters in the exchange interactions (J'/J), crystal field (D/J) and temperature (T=0.0001). **a)** For D/J=0.1, J'/J=1.0, 1.1 and 1.2. **b)** For D/J=1.0, J'/J=1.0, 1.2 and 1.4. **c)** For D/J=1.0, J'/J=0.5, 0.7 and 0.8. **d)** For D/J =1.0, J'/J=0.4 and 0.45. **e)** For D/J=1.0, J'/J=0.33. **f)** For D/J=2.0, J'/J=0.6 and 0.8.

similar to Fig. 4(a) but more complicated from Fig. 4(a). The new phase "C" and new plateaus "1/3, 3/5 and 2/3″ appear in the system. At small values of the J′ more interesting phase and MPs emerge due to stronger frustration, as seen in these figures. (iii) Fig. 5 is constructed in the (D/J, J'/J) plane for h/J=3.0. The MPs stay at the small values of the D/J and J'/J; hence the frustration arises from the competition between the crystal field (D/J) and exchange interaction parameters (J'/J). It is therefore obvious that the crystal field and exchange interactions have very important effects on the MP of the phase diagrams of the model. The crystal field, external magnetic field and exchange interactions are competing each other for constructing the phase regions and MPs on the phase diagrams, but when the values of exchange interaction becomes small the system is more effected by the crystal and magnetic field; hence the new MPs can be obtained for small values of the exchange interaction. The similar result is obtained from the S=1 XXZ model with single-ion anisotropy and large Ising-like anisotropy on a SSL [18]. The effect of the crystal field is also discussed in quantum phase transition of the S=1 S-S model [19].

4. Summary and conclusions

In this paper, we investigated the magnetic properties (MPs, phase diagrams) of a two-dimensional spin-1 Ising model on the SSL in the presence of an external magnetic field within the EFT with correlations. The effects of the applied field on the magnetizations are examined in detail in order to obtain the MPs. In additional to this, different types of MPs such as 1/4, 1/3, 1/2, 3/5, 2/3 and 7/9 of the saturations, are obtained for strong enough magnetic fields, which were found theoretically and also experimentally in a related compound. For example, the MP at m/m_S=1/4, 1/3 and 1/2 was reported in $SrCu_2(BO_3)$ [3,4], at m/m_S=1/3, 1/2 and 7/9 in TbB_4 [7], at m/m_S=1/3 and 3/5 in HoB_4[6], at m/m_S=1/2 in ErB_4 [5,6] and TmB_4 [8]. The MP at m/ms=2/3 was only theoretically denoted the S=1 XXZ model with single-ion anisotropy and large Ising-like anisotropy on a SSL [18]. The ground state phase diagrams are constructed in three different planes, i.e. (h/J, J'/J), (h/J, D/J) and (D/J, J'/J) planes.

Now a brief report is listed as in below:

i. The system exhibits the Néel (N), collinear (C), ferromagnetic (F)

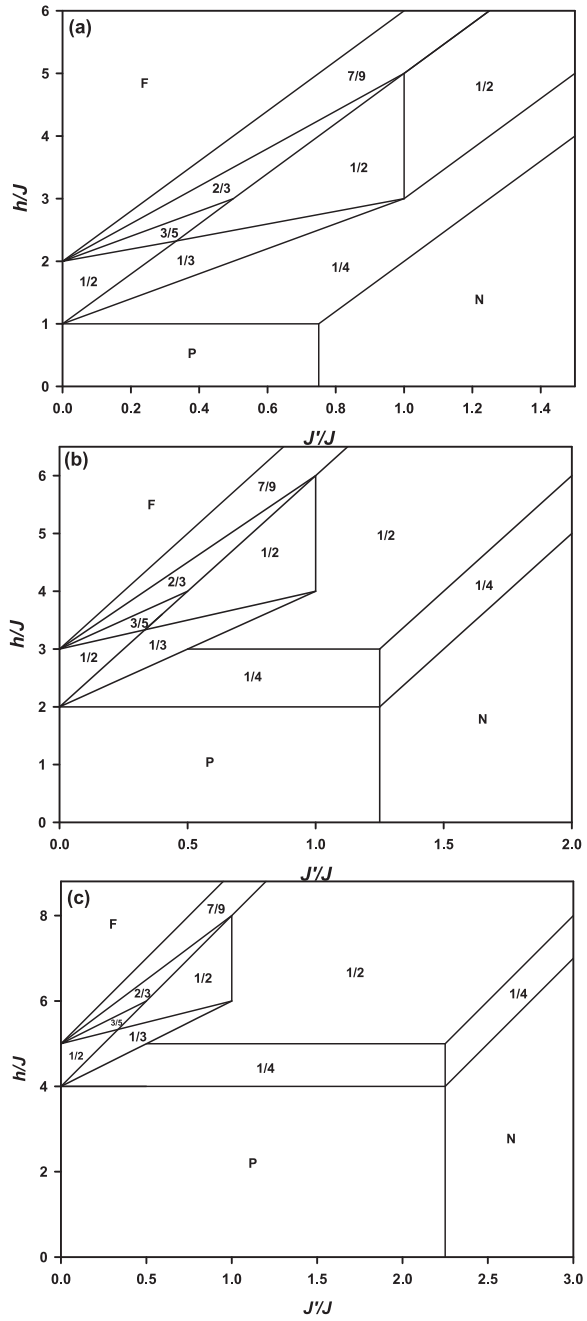

Fig. 3. The ground state phase diagram in the (h/J, J'/J) plane for three different values of D/J, i.e., 1.0, 2.0 and 4.0 for very low values of the temperature, i.e., T=0.0001. **a)**D/J=1.0, **b)**D/J=2.0, **c)**D/J=4.0.

phases, as well as the MP at m/m_S=1/4, 1/3, 1/2, 3/5, 2/3 and 7/9 of the saturation are found for appropriate values of the Hamiltonian parameters.

ii. The system exhibits single (m/m_S=1/2), triple (m/m_S=1/4, 1/2, and 7/9), quintuplet (m/m_S =1/4, 1/3, 3/5, 2/3 and 7/9) and sextuple-plateaus (m/m_S =1/4, 1/3, 1/2, 3/5, 2/3 and 7/9) according to the interaction parameters.

iii. The system exists three 1/2 plateaus having different spin structures i.e. (1,0,1,0); (1,1,0,0) and (0,0,1,1) for D/J=1.0 on the (h/J, J'/J) plane when D/J becomes more strong (D/J=2.0) in addition to this, two 1/4 plateau having different spin structures (at low values of J'/J (1,0,0,0); at high values of J'/J (0,−1,1,1)) are seen.

iv. The MPs start from the higher values of the external magnetic field with the increasing values of the crystal field. It is therefore obvious

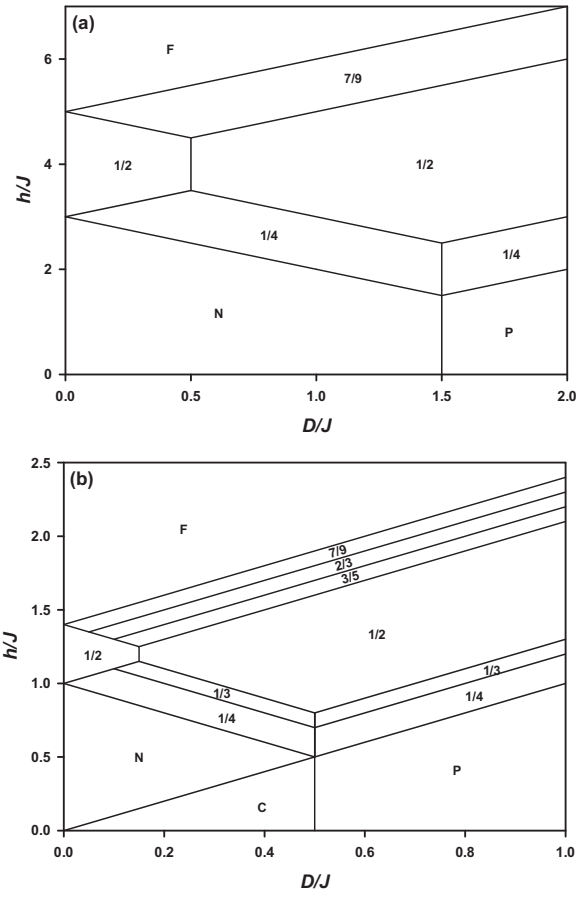

Fig. 4. The ground state phase diagram in the (h/J, D/J) plane for two different values of J'/J, i.e., 1.0 and 0.1 for very low values of the temperature, i.e., T=0.0001. **a)**J'/J=1.0, **b)**J'/J=0.1.

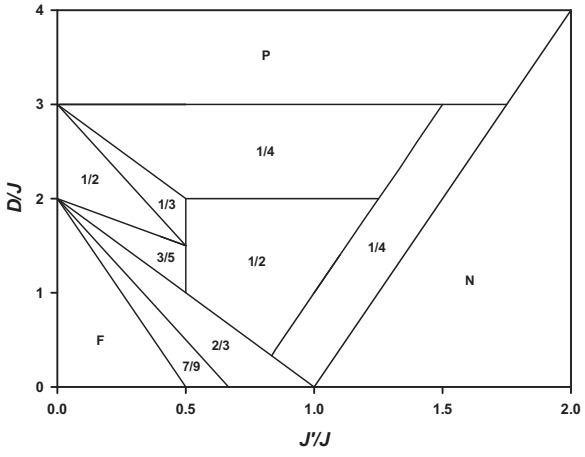

Fig. 5. The ground state phase diagram in the (D/J, J'/J) plane for the values of h/J=3.0 for very low values of the temperature, i.e., T=0.0001.

that the crystal field has a very important effect on the ordering of the phase diagrams of the model. It may be related to strong crystal field causing large energy differences between split-levels.

v. The MPs originate from the competition between the crystal field and interaction parameters.

Finally, we hope that our detailed theoretical investigation may stimulate further works to study the theoretical and experimental researches on the magnetic properties of the frustrated model as well as its magnetism.

References

[1] B.S. Shastry, B. Sutherland, Physica B C 108 (1981) 1069.
[2] R.W. Smith, D.A. Keszler, J. Solid State Chem. 93 (1991) 430.
[3] H. Kageyama, K. Yoshimura, R. Stern, N.V. Mushnikov, K. Onizuka, M. Kato, K. Kosuge, C.P. Slichter, T. Goto, Y. Ueda, Phys. Rev. Lett. 82 (1999) 3168.
[4] K. Onizuka, H. Kageyama, Y. Narumi, K. Kindo, Y. Ueda, T. Goto, J. Phys. Soc. Jpn. 69 (2000) 1016.
[5] S. Michimurea, A. Shigekawa, F. Iga, M. Sera, T. Takabatake, K. Ohoyama, Y. Okabe, Physica B 596 (2006) 378.
[6] S. Matas, K. Siemensmeyer, E. Wheeler, E. Wulf, R. Beyer, Th Hermannsdörfer, O. Ignatchik, M. Uhlarz, K. Flachbart, S. Gabani, P. Priputen, A. Efdokimova, N. Shitsevalova, J. Phys.: Conf. Ser. 200 (2010) 032041.
[7] S. Yoshii, T. Yamamoto, M. Hagiwara, S. Michimura, A. Shigekawa, F. Iga, T. Takabatake, K. Kindo, Phys. Rev. Lett. 101 (2008) 087202.
[8] K. Siemensmeyer, E. Wulf, H.-J. Mikeska, K. Flachbart, S. Gabani, S. Mat'aš, P. Priputen, A. Efdokimova, N. Shitsevalova, Phys. Rev. Lett. 101 (2008) 177201.
[9] M.C. Chang, M.F. Yang, Phys. Rev. B 79 (2009) 104411.
[10] V.V. Slavin, A.A. Krivchikov, Low Temp. Phys. 37 (2011) 1264.
[11] F.Liu, S.Sachdev, arxiv:0904.3018v1
[12] J.J. Feng, L. Huo, W.C. Huang, Y. Wang, M.H. Qin, J.-M. Liu, Z. Ren, Europhys. Lett. 105 (2014) 17009.
[13] W.C. Huang, L. Huo, G. Tian, H.R. Qian, X.S. Gao, M.H. Qin, J.-M. Liu, J. Phys.: Condens. Matter 24 (2012) 386003.
[14] Z.Y. Meng, S. Wessel, Phys. Rev. B 78 (2008) 224416.
[15] S.A. Deviren, J. Magn. Magn. Mater. 393 (2015) 508.
[16] W.S. Lin, T.H. Yang, Y. Wang, M.H. Qin, J.-M. Liu, Z. Reng, Phys. Lett. A 178 (2014) 2565.
[17] S.A. Deviren, B. Deviren, J. Magn. Magn. Mater. 402 (2016) 94.
[18] L. Su, K. Wierschem, P. Sengupta, Phys. Rev. B 89 (2014) 245432.
[19] A. Koga, N. Kawakami, M. Sigrist, J. Phys. Soc. Jpn. 72 (2003) 938.
[20] J. Richter, H.-J. Schmidt, Eur. Phys. J. B 85 (2012) 179.
[21] B. Deviren, E. Kantar, M. Keskin, J. Magn. Magn. Mater. 324 (2012) 2163.
[22] T. Kaneyoshi, J. Magn. Magn. Mater. 336 (2013) 8.
[23] (a) E. Kantar, B. Deviren, M. Keskin, Eur. Phys. J. B 86 (2013) 253;
(b) B. Deviren, Y. Şener, J. Magn. Magn. Mater. 386 (2015) 12.
[24] B. Deviren, Y. Şener, M. Keskin, Physica A 392 (2013) 3969.
[25] M. El Hamri, S. Bouhou, I. Essaoudi, A. Ainane, R. Ahuja, Physica A 443 (2016) 385.
[26] T. Kaneyoshi, J. Phys. Chem. Sol. 87 (2015) 104.
[27] X. Shi, Y. Qi, Physica B 495 (2016) 117.
[28] E. Costabile, J. Ricardo de Sousa, Phys. Rev. E 85 (2012) 011121.
[29] B. Deviren, S. Akbudak, M. Keskin, Sol. State Commun. 151 (2011) 193.
[30] R. Honmura, T. Kaneyoshi, J. Phys. C: Solid State Phys. 12 (1979) 3979.
[31] T. Kaneyoshi, I.P. Fittipaldi, R. Honmura, T. Manabe, Phys. Rev. B 24 (1981) 481.
[32] H.B. Callen, Phys. Lett. 4 (1963) 161.
[33] E.F. Sarmento, C. Tsallis, R. Honmura, Phys. Rev. B 31 (1985) 3153.